

Article

Let's Talk about Sex Hormone Receptors and Their Physical Interaction with Sonic Hedgehog Protein: A Computational Study with Emphasis on Progesterone Receptor

Antonija Tomić ^{1,*}, Josipa Čonkaš ²  and Petar Ozretić ² ¹ Division of Organic Chemistry and Biochemistry, Ruder Bošković Institute, Bijenička 54, 10000 Zagreb, Croatia² Division of Molecular Medicine, Ruder Bošković Institute, Bijenička 54, 10000 Zagreb, Croatia;

jconkas@irb.hr (J.Č.); pozretic@irb.hr (P.O.)

* Correspondence: antonija.tomic@irb.hr

Featured Application: Targeting interaction between sonic hedgehog protein and sex hormone receptors might be a valuable strategy for the treatment of endocrine-resistant tumors.

Abstract: The mature form of the sonic hedgehog protein (SHH-N) is the main canonical activator of the Hedgehog-GLI signaling pathway whose aberrant activity can lead to the development of hormone-dependent cancers like breast or prostate cancer. In this study, we employed computational methods to explore the potential binding of SHH-N with the progesterone receptor (PR), the sole member of the nuclear sex hormone receptor (SHRs) subfamily not previously linked to SHH-N. Through a combination of molecular docking, robust molecular dynamics (MD) simulations, and free energy calculations, we predicted a stable binding between SHH-N-cholesterol and PR. To validate our findings, we extended our in silico investigation to encompass the complexes between SHH-N-cholesterol and estrogen receptor alpha (ER α) and androgen receptor (AR)—complexes that have been experimentally confirmed in our prior studies. The calculations not only confirmed the stable binding of SHH-N-cholesterol with both ER α and AR but also revealed the strongest binding occurred with ER α , followed by AR and PR, suggesting a non-canonical interaction with potential biological significance. Microsecond-long MD simulations unveiled tight cholesterol binding in the SHRs' binding sites, and we gained insights into sub-molecular interactions contributing to protein-protein stabilization in complexes involving PR and ER α for the first time. The MM/PBSA calculations indicated comparable binding affinities of PR for progesterone and SHH-N-cholesterol, with ER α exhibiting a more favorable enthalpy of binding with SHH-N-cholesterol than with estradiol.

Keywords: sex hormone receptors; progesterone receptor; Hedgehog-GLI; sonic hedgehog; protein-protein docking; protein-protein interactions; molecular dynamic simulations



Citation: Tomić, A.; Čonkaš, J.; Ozretić, P. Let's Talk about Sex Hormone Receptors and Their Physical Interaction with Sonic Hedgehog Protein: A Computational Study with Emphasis on Progesterone Receptor. *Appl. Sci.* **2024**, *14*, 562. <https://doi.org/10.3390/app14020562>

Academic Editor: Francesco Cappello

Received: 13 December 2023

Revised: 3 January 2024

Accepted: 5 January 2024

Published: 9 January 2024



Copyright: © 2024 by the authors. Licensee MDPI, Basel, Switzerland. This article is an open access article distributed under the terms and conditions of the Creative Commons Attribution (CC BY) license (<https://creativecommons.org/licenses/by/4.0/>).

1. Introduction

The evolutionary highly conserved Hedgehog-GLI (HH-GLI) signaling pathway plays an essential role in many aspects of embryonic development, and in adult organisms is mainly responsible for stem cell maintenance and tissue homeostasis [1]. In mammals, the main representatives of the pathway are three hedgehog ligands: desert, Indian, and sonic hedgehog (DHH, IHH, and SHH, respectively); two transmembrane receptors (PTC1 and PTC2); the transmembrane G protein-coupled co-receptor SMO; and a family of transcriptional factors GLI that are regulated by a suppressor of fused (SUFU) protein [2]. The binding of one HH ligand to PTC receptor terminates its repression of SMO and this de-repression causes the release of GLIs from SUFU. GLIs are then translocated to the nucleus, where they regulate the transcription of target genes that are involved in many cellular processes, such as cell cycle regulation and proliferation, cell survival and self-renewal, cell

adhesion, epithelial-mesenchymal transition, angiogenesis and pathway autoregulation [3]. Described activation is considered as ligand-dependent canonical signalization.

HH proteins are morphogens and as such control numerous processes during embryonic development. All HH proteins expressed in mammals are thought to have similar physiological functions, and differences in their roles during development arise from different expression patterns [4]. SHH, however, is the most widely expressed compared to others and is considered to be the main ligand. After translation, HH proteins undergo several processing steps that result in an active ligand. HH proteins contain an N-terminal signaling domain and a C-terminal auto-processing domain. To become fully active, the C-terminal domain autocatalytically initiates cleavage of the protein and addition of cholesterol to the C-terminus of the signaling domain. Furthermore, hedgehog acyltransferase (HHAT) binds the palmitoyl group to the N-terminus of the signaling domain. The mature signal peptide is often designated as HhNp or, in the case of SHH, as SHH-N [5]. These two lipid posttranslational modifications (PTMs) are essential for both the activity and the regulation of HHs spread through tissues [6,7].

Aberrant activation of the HH-GLI pathway in adult cells, caused by either genetic [8] or epigenetic [9] factors, has been linked with the development of various tumor types, including hormone-sensitive cancers, like breast, ovarian, uterine or prostate cancer [10–13]. Hormone-sensitive or hormone-dependent cancers are those whose growth and survival are dependent on hormones that bind to their specific receptors. Both endogenous and exogenous hormones drive cell proliferation and increase the number of cell divisions, resulting in the growth and spread of tumor cells [14]. These four aforementioned cancers are the main types of hormone-sensitive cancers, and they depend on sex steroid hormones—estrogens, progestogens, or androgens. One of the main reasons why tumor cells are hormone-sensitive is because they often overexpress sex hormone receptors (SHRs) in particular, along with estrogen receptors (ER), progesterone receptors (PR), or androgen receptors (AR), which attests to their fundamental role in the pathogenesis and progression of hormone-dependent tumors [15].

SHRs, and specifically their nuclear forms, belong to the steroid hormone receptor subfamily of the nuclear receptor superfamily. They are transcription factors and their structural domains enable affinity binding to both their ligands (sex hormones) and response elements of their target genes, which enables a direct regulation of target gene transcription [16]. SHRs regulate the transcription of genes that control many different biological processes, like cell proliferation, development, metabolism, and reproduction [17].

In one of our previous studies of the role of HH-GLI signaling pathway in breast cancer (BC), we found that SHH co-localize with estrogen receptor alpha (ER α) in the ER-positive BC cell line MCF-7, but not in the ER-negative cell line SK-BR-3 [18]. Since cholesterol is a precursor to all sex steroid hormones (Figure 1) [19], we have started to hypothesize that SHH-N could physically interact, through its cholesterol PTM, with SHRs, and activate their signaling pathways (i.e., achieve transcription of their target genes). In our more comprehensive study of the role of the HH-GLI signaling pathway in prostate cancer (PC), we have proven, both experimentally and computationally, that in the androgen-dependent prostate cancer cell line LNCaP, which was made androgen-independent, SHH-N non-canonically binds to AR and activates it, and thus sustains androgen-independent PC cell growth [20]. Furthermore, inhibition of this interaction by statins, the cholesterol-lowering drugs, led to AR signaling downregulation, and this might offer a valuable, new strategy for the treatment of advanced (or so-called “castration-resistant”), androgen-independent, or hormone-refractory PC.

Considering all available knowledge, progesterone receptor (PR) remains the only member of the nuclear SHRs without any indication of its potential interaction with SHH. Like all the other SHRs, PR acts as a ligand-dependent transcription factor—when activated with progesterone, it regulates gene expression, influencing cell growth, proliferation and differentiation, and other functions. Two PR isoforms, PRA and PRB, are described in humans, where PRB is considered as the canonical isoform, and has 164 amino acids longer

N-terminus known as the “B-upstream segment” [21]. Both isoforms have similar levels of expression in normal tissues, and their ratio can be altered in BC with a poor prognosis, where the loss of PRB and predominance of PRA are present [22]. Furthermore, with the exception of BC and gynecologic cancers, altered PR expression has also been described in some other non-gynecologic cancers, such as astrocytomas, pituitary adenomas, colorectal and thyroid carcinomas [23–26]. The presence and activity of PR in tumors can influence their response to hormonal therapies, affecting the prognosis and treatment strategies [27]. In some cases, higher expression of PR might protectively affect tumor development and progression, particularly in hormone-sensitive cancers, like certain subtypes of ovarian cancer, endometrial tumors, and Grade 1 meningiomas [28–30], where PR signaling can inhibit uncontrolled cell growth and proliferation or is associated with a significantly more favorable prognosis. However, the impact of PR in various tumor types can differ based on the specific biological characteristics and signaling pathways involved in the particular tumor type.

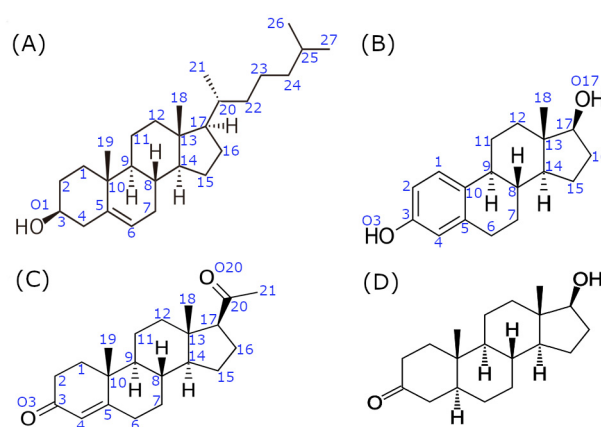


Figure 1. Comparative molecular structures of cholesterol and its sex hormone derivatives, the most potent natural agonists of their respective receptors. (A) cholesterol; (B) estradiol (E2); (C) progesterone (P4); (D) 5 α -dihydrotestosterone (DHT). Blue numbers indicate the respective positions of carbon and oxygen atoms referenced throughout the text.

In this study we conducted comprehensive molecular docking and molecular dynamics studies to find both binding affinities and molecular modes of interaction between cholesterol moiety of SHH-N and all three types of sex hormone receptors, with particular emphasis on PR. In establishing positive controls for docking studies we used structures of the most potent natural agonists of the respective receptors, which are presented in Figure 1. Free cholesterol was also used as a control molecule to deduce if/how the protein backbone of SHH-N affects the interaction between cholesterol and SHRs.

2. Materials and Methods

2.1. System Preparation

The ER α -estradiol complex was built from the X-ray structure of the human ER α ligand-binding domain in complex with 17 β -estradiol deposit in PDB under code 1ERE (chain A, resolution 3.10 Å) [31]. Missing residues 331–336 and 462–464 in the human ER α ligand-binding domain structure were modelled using a Swiss-model server (<https://swissmodel.expasy.org/> (accessed on 30 March 2023)) [32] and a structure deposit, under PDB code 1ERE, as templates. The modelled ER α ligand-binding domain structure was used for building the ER α -cholesterol complex, and cholesterol was bound in the same position as estradiol by aligning their tetracyclic rings (i.e., gonane cores). The structure of the progesterone-bound human PR ligand-binding domain deposit under code 1A28 (chain A, resolution 1.80 Å) [33] was used for PR-progesterone complex simulations. In

addition, this structure was used for building up the PR–cholesterol complex structure after the alignment of cholesterol and progesterone gonane cores.

2.2. Molecular Docking and Molecular Modeling Details

Protein-protein (PP) complexes between the C-terminally cholesteroylated N-terminal domain of SHH (SHH-N-cholesterol; PDB code 6RVD, chain C, resolution 3.5 Å) [34] and the ER α , PR or AR ligand-binding domain (PDB code 2AM9, chain A, resolution 1.64 Å; further in text AR) [35], so-called ER α –SHH-N-cholesterol, PR–SHH-N-cholesterol and AR–SHH-N-cholesterol complexes (respective order), were also built. The cholesterol molecule attached to the SHH-N C-terminal in the complexes with the ER α and PR proteins was bound in the same position as determined for cholesterol alone in the aforementioned complexes. The position of the cholesterol moiety bound to the SHH-N C-terminal in the complex with AR was determined by superimposing the structure of AR with ER α from the complex with SHH-N-cholesterol. Mutual orientation of SHH-N and ER α , PR or AR proteins in the PP complex was determined by performing a docking study with the Hdock server (<http://hdock.phys.hust.edu.cn/> (accessed on 13 April 2023)) [36]. More specifically, ER α (chain A from PDB code 1ERE), PR (chain A from PDB code 1A28) or AR (chain A from PDB code 2AM9) were selected as receptor molecules, and the N-terminal domain of SHH (chain C from PDB code 6RVD) was selected as a ligand molecule for predicting the ER α –SHH-N, PR–SHH-N or AR–SHH-N complex structures (respective order) by applying the Hdock server. The E353 residue of ER α , Q725 residue of PR or Q711 residue of AR and G197 residue of SHH-N (residue covalently bonded to cholesterol moiety) were selected as binding site residues in order to identify PP binding poses that could allow binding of cholesterol moiety at the cholesterol binding site. No complex structure with direct interaction between E353–G197 residues in the ER α –SHH-N complex, Q725–G197 residues in the PR–SHH-N complex or Q711–G197 residues in the AR–SHH-N complex, was obtained, as the unstructured C-terminus of the SHH-N protein closely interacts with a protein surface (Figure S1). However, in a few (2–3 out of top 10) identified complex poses (Figure S2), the cholesterol moiety at C-terminus of SHH-N could bind in the cholesterol binding site of ER α , PR or AR after slight modification, i.e., after detachment of SHH-N unstructured C-terminus from the adjacent alpha helix (residues Q100–N115). This was accomplished by manually changing the dihedral angles of the amino acid residues from the unstructured SHH-N C-terminus. For the further modelling study, one binding pose for each complex structure was selected (more precisely the one that required the least intervention in the C-terminus of the SHH-N protein to allow binding of cholesterol moiety in a position that most closely resembles the one in the complex with cholesterol alone).

The complexes were solvated in an octahedron box filled with OPC water molecules [37], ensuring an 11 Å thick water molecules buffer around the protein. The Cl[−] ions were added to neutralize the system. All Arg and Lys residues in the structures were positively charged (+1e), and Glu and Asp residues were negatively charged (−1e) as expected at physiological conditions. The histidines were in a neutral state with a proton at the N ϵ atom, except for the H140 of SHH-N, H398 of ER α and H689 of AR, which were in a neutral state with a proton at the N δ . The obtained complex was parametrized by the AmberTools20 module tleap, using a ff19SB force field [38]. Cholesterol and estradiol were parametrized within the gaff force field [39] and AM1-BCC charges were assigned. For the zinc cation, non-bonded parameters that we developed were used [40].

2.3. MD Simulations Details

Prior to MD simulations, the protein geometry was optimized in three cycles with different constraints. In the first cycle (2500 steps), only water molecules and ions were relaxed, while the protein and ligand (cholesterol (moiety), progesterone and estradiol) were restrained by the harmonic potential with a force constant of 32 kcal mol/Å²; in the second (2500 steps) cycle, the force constant of 12 kcal mol/Å² was applied to the protein backbone; and in the third cycle (4500 steps), all atoms were free to move. Followed heating

(250 ps, protein and ligand were restrained with a force constant of 10 kcal mol/Å²), density equilibration (1 ns, protein backbone and ligand were restrained with a force constant of 10 kcal mol/Å²) and productive MD simulation. During heating from 0 to 300 K, the NVT ensemble was used, while density equilibration and productive MD simulations were performed using a *NpT* ensemble. The temperature (300 K) was held constant using Langevin dynamics [41], with a collision frequency of 1 ps⁻¹. Pressure was regulated by using a Berendsen barostat [42]. The time step was 1 fs during equilibration and 2 fs during productive MD simulations. Bonds involving hydrogen atoms were constrained by using the SHAKE algorithm. Simulations were performed with the GPU version of the pmemd (pmemd.cuda) program [43,44] from the AMBER software suite version 20 (<https://ambermd.org/> (accessed on 1 April 2021)) [45], using periodic boundary conditions (PBC) with a cutoff value of 11 Å, and the particle mesh Ewald (PME) method was used to calculate the long-range electrostatic interactions. The 0.5 μs-long MD simulations were performed for ERα and PR in complexes with their natural agonist (estradiol and progesterone, respectively) and cholesterol, as well as AR in a complex with the SHH-N-cholesterol protein. The SHH-N-cholesterol in a complex with ERα and PR was subjected to microsecond-long MD simulations. More precisely, in order to obtain a stable complex structure, the ERα-SHH-N-cholesterol complex was subjected to 2 μs-long MD simulation. In the case of the PR-SHH-N-cholesterol complex, two 1 μs-long MD simulations were conducted (designated as simulations a and b). Notably, the first half of both simulations was identical; the structure sampled after 0.5 μs was used as the starting structure for two additional independent 0.5 μs-long MD simulations, employing different seed numbers.

2.4. MM/G(P)BSA Calculations

The enthalpy contributions to the free energies of binding of the different ligands (estradiol, progesterone, cholesterol or SHH-N-cholesterol) with AR, PR or ERα were calculated by using the MM/PBSA (Molecular Mechanics Poisson-Boltzmann Surface Area) [46] approach implemented in the AMBER 20 program. Calculations were performed for the protein with dielectric constant 2.0 immersed in the solvent with dielectric constant 80. The ion concentration was 0.1 M. The polar component of the enthalpy of solvation was calculated by applying the Poisson-Boltzmann method and the nonpolar component was determined by $\Delta H_{\text{nonpol}} = \gamma \text{SASA} + \beta$, where the surface area accessible by the solvent (SASA) was calculated using the MolSurf program [47]. The surface tension γ and the offset β were set to the standard values of 0.0378 kcal (mol Å²)⁻¹ and 0.5692 kcal/mol, respectively.

To elucidate the differences in binding energies and identify the residues critical for protein-protein and protein-ligand binding, the free energy of binding was decomposed into the contribution of each residue by using the MM/GBSA (Molecular Mechanical Generalized Born Surface Area) approach implemented in the AMBER 20 software. Residue-based MM/GBSA free energy analysis was performed to highlight the residues relevant to the stabilization of the protein-ligand and protein-protein complexes. Calculations were performed for the enzyme with a relative permittivity of 1.0 immersed in a solvent with a relative permittivity of 80.0.

The MM/PBSA binding energy calculations were performed on the different time intervals obtained throughout the MD trajectory, considering structures sampled every 40 ps. The per-residue based MM/GBSA calculations were performed on the (last) 0.5 μs-long time intervals obtained from MD simulations, except for ERα-SHH-N-cholesterol complex, where the last 600 ns (from 1.4th till 2nd μs) were considered. Herein, structures sampled every 200 ps were analyzed. We calculated the contribution of enthalpy to binding free energy, since conformational entropy is usually neglected due to its high computational cost when only the relative binding free energies of similar ligands are needed.

2.5. Analysis

RMSD (root-mean-squared deviation), R_g (radius of gyration), per-residue RMSF (root mean square fluctuation) and selected amino acid distances were calculated with AMBER's

cpptraj module. In addition, native and non-native contacts were calculated by using the cpptraj module within the AMBER20 program. Hydrogen bond analysis was performed by using the HBonds plugin for VMD (<http://www.ks.uiuc.edu/Research/vmd/plugins/hbonds/> (accessed on 15 October 2023)).

3. Results

A molecular modeling study was conducted to explore the potential binding of C-terminally cholesteroylated N-terminal domain of SHH with SHRs. Herein, the main focus was on the binding of SHH-N-cholesterol with PR, as interaction with ER α and AR has already been confirmed [18,20]. While there is experimental evidence supporting the existence of the ER α -SHH-N-cholesterol complex, the specific molecular interactions within it remain unclear. In contrast, a computational study of the AR-SHH-N-cholesterol complex has been conducted previously. However, in this study, we repeated these simulations using a more up-to-date force field and water model compared to those utilized in the previous investigation [20], allowing for a meaningful comparison with the newly obtained results. MD simulations of ER α and PR in complexes with their most potent natural agonist (ER α -estradiol and PR-progesterone complexes, respectively), were used as a positive control.

We lacked prior knowledge about the residues involved in PP interactions between SHR and SHH-N, and so conducted a PP docking study by using the Hdock server to predict binding complexes between two proteins. The most geometrically compatible PP complexes obtained by docking were subjected to robust MD simulations and binding free energy calculations. The results of these studies enabled us to investigate which non-canonical interaction of SHR with C-terminally cholesteroylated N-terminal domain of SHH is more likely.

3.1. Complexes with Estradiol and Progesterone

Complexes in which estradiol and progesterone were bonded with ER α and PR, respectively, remained stable during simulations (see protein RMSD and Rg profiles in Figure S3), with no significant change in the orientation of the ligand molecules in the rather tight binding pocket of the receptor proteins (Figure S4). Ligands' RMSF profiles indicate low fluctuations of estradiol and progesterone heavy atoms during the production phase (Figure 2).

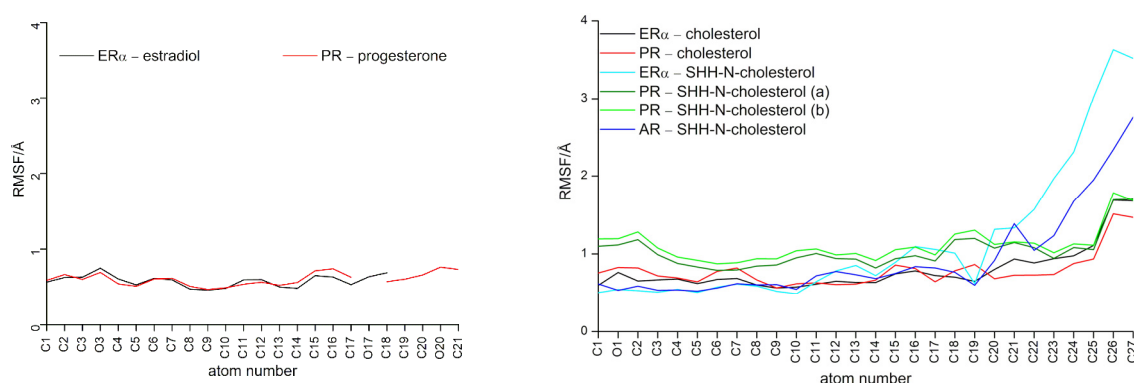


Figure 2. Ligands' heavy atoms RMSF profile calculated throughout the entire MD simulation after RMSD alignment of the ER α , PR or AR backbone to the first structure obtained from the production phase was performed. The O1 atom of cholesterol is covalently bonded with G197 residue from the SHH-N C-terminal. Atom names are indicated in Figure 1.

Strong hydrogen bonds formed between the hydroxyl groups (oxygen atoms O3 and O17) of estradiol and E353 and H524 residues of ER α , and the carbonyl groups (oxygen atoms O3 and O20) of progesterone and R766, Q725 and C891 residues of PR, greatly contributing to ligand stabilization in the interior of the protein during simulations

(Figure S5). Interestingly, salt bridge interaction between E353 and R394 residues of ER α found at the entrance to the ligand binding site, and present in the ligand-free protein structure (e.g., in ER α structure deposit under PDB code 2B23), is mostly preserved upon complexation (Figure S6). By referring to overlaying SHR structures it can be seen that amino acids Q725 and R766 in PR protein (and Q711 and R752 in AR protein) are located at the equivalent position as E353 and R394 in ER α . Although intra-molecular hydrogen bonds between Q725 and R766 residues of PR rarely form in complexes with progesterone (Figure S6), they more frequently engage in inter-molecular hydrogen bonding with progesterone (Figure S5).

In addition to these hydrogen bonding interactions, the MM/GBSA per-residue analysis highlights the importance of non-polar amino acid residues of ER α (L346, A350, L387, M388, L391, F404, M421, and L525) and PR residues (L715, L718, L721, Q725, M756, M759, V760, L763, R766, F778, L887, and Y890) in the stabilization of the gonane core of estradiol and progesterone (respectively) within the interior of the receptor binding site (residues indicated with red dots in Figure 3 and depicted in Figure 4).

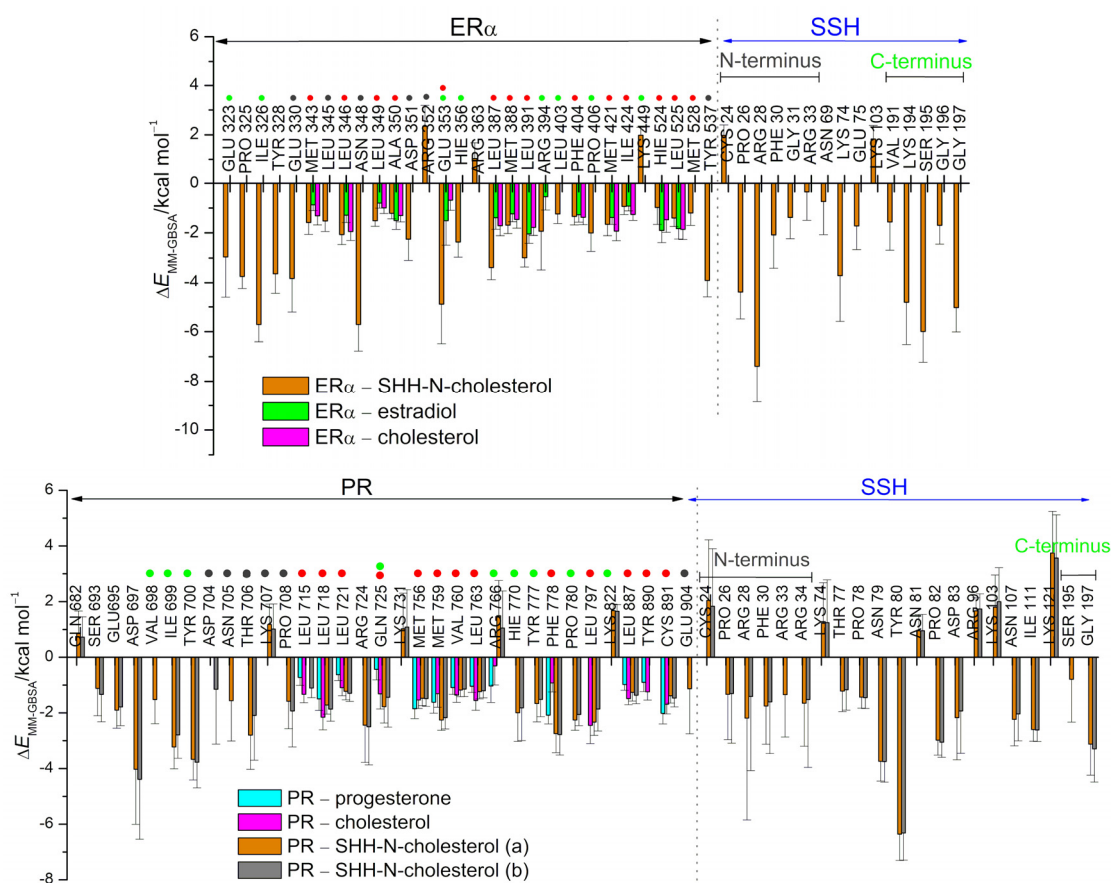
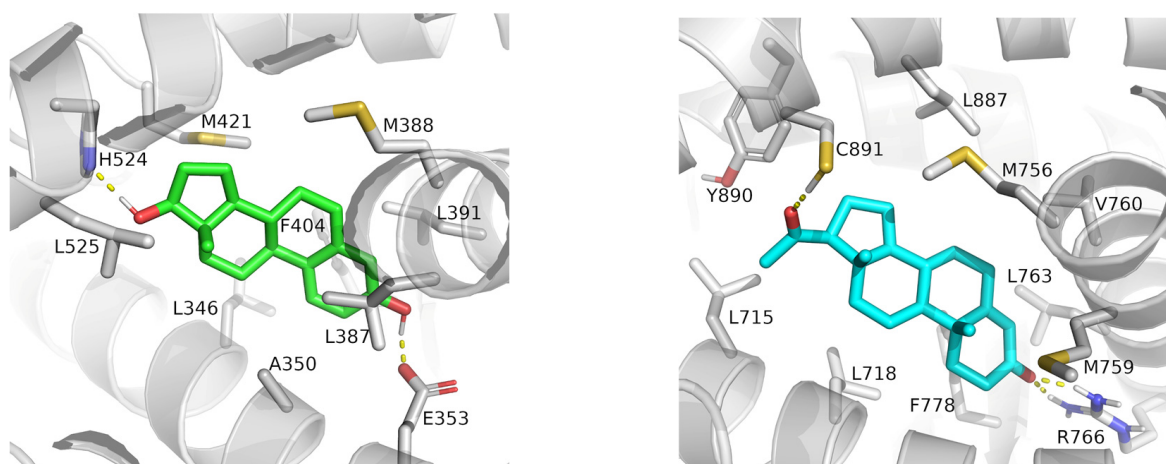


Figure 3. The MM/GBSA per-residue energy decomposition was performed for ER α , PR, and SHH-N proteins in the studied complexes. The energies were calculated based on 0.5 μ s-long MD simulations for complexes with sex steroid hormones and cholesterol. For complexes involving SHH-N, the last 0.5 and 0.6 μ s-long trajectories were considered, corresponding to complexes with PR and ER α , respectively. Values are given for residues with energy contributions larger than ± 1.5 kcal/mol. The amino acid residues from the unstructured N- and C-terminus of SHH-N protein (residues C24-K45 and V185-G197, respectively) are indicated. Residues highlighted with a red dot interact with estradiol, progesterone or cholesterol (moiety), while residues highlighted with a green or gray dot interact with unstructured C- or the N-terminus of the SHH-N protein, respectively. The Glu353 residue of ER α and Gln725 residue of PR have red and green dots assigned, as in complexes with SHH-N-cholesterol they interact both with sterols and the SHH-N C-terminus.

ER α -estradiol

PR-progesterone

Figure 4. Binding of estradiol (green) and progesterone (cyan) with ER α and PR (SHR proteins in light gray), respectively, in the optimized structures obtained after 0.5 μ s of simulation. Residues that, according to per-residue MM/GBSA analysis (Figure 3), interact with the ligand are indicated. Non-polar hydrogens and main chain atoms are not shown. Hydrogen bonds are indicated as yellow dashed lines.

3.2. SHRs in Complex with SHH-N-Cholesterol (PP Complexes)

The RMSD profiles of individual proteins within the PP complexes (red and green curves in Figure S3, left) indicate that protein structures remained preserved during MD simulations. Furthermore, the globularity of each protein (ER α , PR, AR or SHH-N-cholesterol) has not changed during the production phase (red and green curves in Figure S3, middle). Similarly, the RMSD and R_g profiles calculated for the entire PR-SHH-N-cholesterol and AR-SHH-N-cholesterol complexes suggest that these structures remained stable throughout the production phase, showing minimal deviation from their initial configurations (black curves in Figure S3, left and middle, and Figures S7 and S8). The final PR-SHH-N-cholesterol complex structures derived from two separate 1 μ s-long MD simulations are almost identical (Figure 5a), with RMSD of C α atoms (not considering SHH-N unstructured N- and C-termini) of 1.22 Å (see structures show in Figure 5b). This indicates the high stability of the PR-SHH-N-cholesterol, as well as AR-SHH-N-cholesterol, complex structure initially predicted by docking. The alignment of the final structure of the AR-SHH-N-cholesterol complex obtained in this study with those from our previous work [20] reveals the formation of similar PP complexes (see Figure S9). The most notable difference lies in the position of the SHH-N-cholesterol N-terminus, which is shown to be the most flexible part of the protein (as discussed below). The consistent binding energies calculated throughout the production phase, as outlined in Table 1 for each complex, further affirm the stability of the initially predicted PR-SHH-N-cholesterol and AR-SHH-N-cholesterol complex structures.

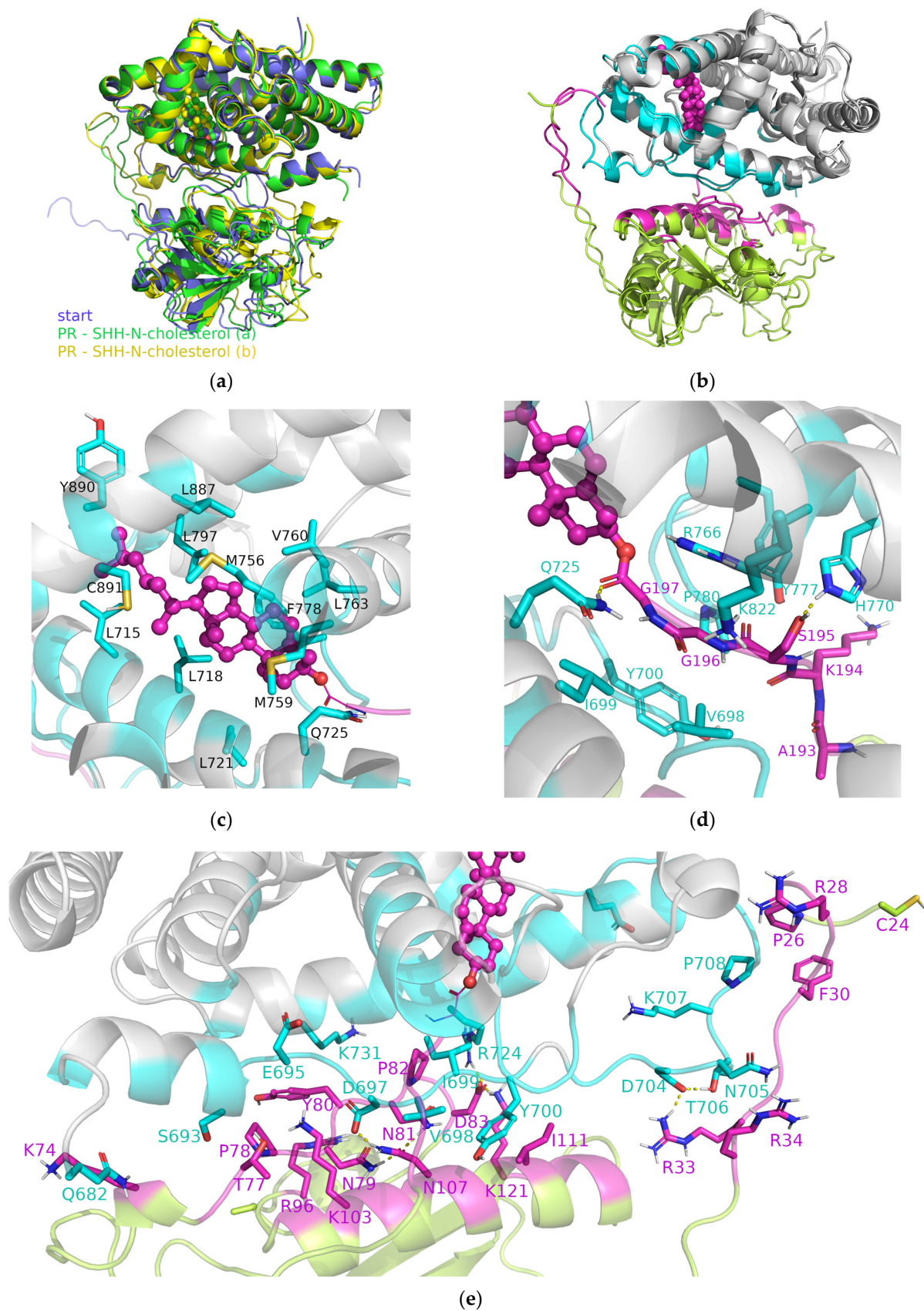


Figure 5. The PR-SHH-N-cholesterol structures obtained from the molecular modeling study: (a) aligned structures obtained by the Hdock server (violet) and after 1 μ s of MD simulations (green and yellow), (b) aligned optimized complex structures obtained after 1 μ s of MD simulations, where PR

is colored in gray, and SHH-cholesterol in lime. Furthermore, residues of SSH-N-cholesterol found within 4 Å of PR are colored magenta, and residues of PR found within 4 Å of SHH-N-cholesterol are colored cyan. In the middle and bottom rows, an enlarged view is provided, highlighting the residues that, based on per-residue MM/GBSA analysis, contribute to the complex stabilization. More precisely, PR residues that: (c) interact with cholesterol moiety, (d) stabilize binding of the unstructured C-terminus of SHH-N, and (e) stabilize binding of the unstructured N-terminus of SHH-N, as well as its more structured central part, are shown. Hydrogen bonds are indicated with a dashed yellow line. Non-polar hydrogen atoms are not shown. Cholesterol moiety is shown as a sphere (and sticks) and colored magenta in (b–e).

Table 1. The enthalpy contribution to the binding free energies, calculated based on MD trajectories of the simulated systems by using the MM/PBSA approach. The specific time intervals subjected to analysis are indicated.

Complex	Time Interval/ns	($\Delta H_{\text{bind}} \pm \text{SD}$)/(kcal/mol)
ER α -estradiol		-12.87 ± 2.68
ER α -cholesterol		-17.50 ± 3.42
PR-progesterone	0–500	-19.02 ± 2.97
PR-cholesterol		-19.48 ± 3.63
PR-SHH-N-cholesterol	0–500	-23.53 ± 8.33
	300–500	-20.99 ± 7.14
	500–1000 (a) *	-27.95 ± 7.80
	500–1000 (b) *	-23.25 ± 7.66
AR-SHH-N-cholesterol	0–500	-33.03 ± 10.27
	300–500	-29.73 ± 11.09
ER α -SHH-N-cholesterol	0–300	-20.70 ± 7.28
	300–500	-40.12 ± 9.25
	600–800	-45.56 ± 9.5
	800–1000	-36.29 ± 8.66
	1100–1350	-42.40 ± 8.45
	1400–2000	-51.51 ± 7.30

* Two separate 1 μs -long MD simulations of the PR-SHH-N-cholesterol complex are designated as a and b.

During MD simulations, a significant structural deviation from its initially docked configuration was observed in the ER α -SHH-N-cholesterol complex, as evidenced by the complex RMSD profile (black curve in Figure S3, middle). This structural rearrangement can be described as a shift in the mutual orientation of individual proteins (see Figures S7 and S8). The reorganization of protein subunits is concomitant with changes in binding energies (refer to Table 1). Specifically, after 300 ns of MD simulations, the energy of the ER α -SHH-N-cholesterol complex becomes more negative, signifying an increase in binding affinity. The most stable complex is formed after 1.4 μs of MD simulation (Table 1). During the last 0.6 μs of the MD simulation, the structure of the ER α -SHH-N-cholesterol complex remains mostly unchanged (Figures S3 and S7). Interestingly, during this timeframe, the relative orientation of SHH-N to ER α closely resembles its position in complexes with AR and PR (Figure S8). According to the R_g profiles (black curves in Figure S3, middle), complexes formed between AR or PR and SHH-N-cholesterol are slightly more globular than the complex formed between ER α and SHH-N-cholesterol (see the final complex structures in Figure S8). This is further evident from the reduced number of amino acids from the central, more structured, part of the SHH-N protein that contribute to the stabilization of the complex with ER α , compared to AR and PR (as discussed below).

To conclude, MD simulations suggest the possibility of a stable complex forming between the C-terminally cholesteroylated N-terminal domain of SHH and all three SHRs (ER α , PR and AR). In addition, MM/PBSA energies (Table 1) indicate that the binding of the N-terminal domain of SHH-N with covalently bound cholesterol to ER α is found to be more

exothermic ($\Delta H_{\text{bind}} = -51.51 \pm 7.30$ kcal/mol for the last 0.6 μs), when compared to binding with AR ($\Delta H_{\text{bind}} = -33.03 \pm 10.27$ kcal/mol) and PR ($\Delta H_{\text{bind}} = -27.95 \pm 7.80$ kcal/mol for the last 0.5 μs). Notably, when considering standard deviations, the binding enthalpies for AR and PR are similar.

During MD simulations, cholesterol, whether free or attached to the C-terminus of SHH-N, remained tightly bound within the SHRs binding site, occupying a similar binding position as in the initial structure (illustrated in Figure S4), which was determined through the binding of its natural agonists. Ligands' RMSF profiles indicate higher mobility only for the cholesterol's aliphatic side chain atoms (atoms C25–C27, see Figure 2). According to per-residue MM/GBSA analysis, cholesterol gonane core is within the SHR binding site mostly stabilized by the same amino acid residues as identified for estradiol or progesterone in the complex with ER α and PR, respectively (see Figures 3 and S10), wherein cholesterol's aliphatic side chain atoms are stabilized by M343, M421, I424, H524 and L525 residues in the ER α –(SHH-N)-cholesterol complex, and L715, L797, L887, Y890 and C891 residue in the PR–(SHH-N)-cholesterol complex (depicted in Figures 5c and S11). The significance of van der Waal's interactions in ligand stabilization is emphasized by the substantial energy contribution from the H524 residue of ER α and the C891 residue of PR to cholesterol binding. Specifically, according to MM/GBSA analysis (Figure 3), these residues interact with cholesterol as strongly as they do with estradiol or progesterone. However, in complexes with the latter, hydrogen bonding with these residues predominantly contributes to ligand stabilization, while in complexes with cholesterol, van der Waal's interactions with these amino acids play a key role in stabilizing ligand binding. A salt bridge interaction between E353 and R394 residues, located at the entrance to the ER α buried binding site, is observed in the complex with SHH-N, as in the complex with estradiol (Figures S6 and S12). However, in the ER α –SHH-N-cholesterol complex, E353 does not form a hydrogen bond with the hydroxyl group of the cholesterol molecule (oxygen atom O1), as it does with the hydroxyl (O3) group of estradiol (Figure S5). Instead, it more frequently engages in hydrogen bonding with the amino acid residues from the unstructured C-terminus of the SHH-N protein (Figure S13, middle). In complexes with PR, residues Q725 and R766 (found at the entrance to the PR binding site) are more frequently engaged in hydrogen bonding with the ligand (Figures 5d and S5) than with each other (Figures S6 and S12). Similar to the complex with progesterone, R766, and frequently Q725, residues make a hydrogen bond with the hydroxyl group of the cholesterol molecule (oxygen atom O1) that corresponds to carbonyl (O3) groups of progesterone, but also with amino acid residues from the unstructured C-terminus of the SHH-N protein (Figures 5d and S12). Residues R572 and Q711 from AR also make hydrogen bonds with amino acid residues from the unstructured C-terminus of the SHH-N protein (Figures S12 and S13). A higher number of hydrogen bonds between these residues near the entrance of the SHRs' binding site and the C-terminus of SHH-N is observed in the complex with ER α , than with PR and AR (Figure S12). In addition to the aforementioned hydrogen bonds, the per-residue MM/GBSA analysis identified other residues from SHRs that interact with the tetra-peptide motif K194-G197 at the C-terminus of SHH-N and contribute to PP complexes stabilization (highlighted with green dots in Figures 3 and S10). Favorable interactions involve receptor residues E323, I326, E353, H356, R394, L403, and P406 in the complex with ER α ; V698, I699, Y700, Q725, H770, Y777, and P780 in the complex with PR; and E681, Q711, A748, W751, R752, and T755 in the complex with AR.

Apart from the residues from the unstructured C-terminus of SHH-N, which are in direct contact with SHR due to cholesterol binding in the interior of the receptor, the unstructured N-terminus and the more structured central part of the SHH-N protein also participate in the formation of stable PP complexes with ER α , AR or PR (Figures 3 and S10). According to MM/GBSA analysis, the residues from the structured central part of the SHH-N protein that stabilize PP complexes are: N69, K74 and E75 in the complex with ER α ; T77, P78, N79, Y80, P82, D83, N107 and I111 in the complex with PR; and Y80, P82, D83, Q100, A108 and I111 in the complex with AR (Figures 3 and S10). Residues within SHRs

that establish favorable interactions with SHH-N include: P325 and Y328 of ER α ; S693, E695, D697, Y700 and R724 of PR; and V676, A679 and V685 of AR (Figures 3 and S10). It can be noticed that chemically different amino acid residues contribute to the stabilization of the PP complex, and that more amino acids from the central part of the SHH-N protein contribute to the stabilization of the complex with PR and AR, than ER α . As expected, MD simulation indicated that the most flexible part of the SHH-N-cholesterol protein in PP complexes is its N-terminus (Figure S7). During the simulation, the N-terminus stabilizes by binding to the SHRs, establishing interactions with E330, L345, N348, D351 and Y537 residues in the complex with ER α ; D704, N705, T706 and E904 residues in the complex with PR; and D690 residue in the complex with AR (Figures 3 and S10). The lowest number of amino acids from AR that interact with the N-terminus of SHH-N, as identified by per-residue MM/GBSA analysis, indicates the highest flexibility of that region in the complex with AR (see Figure S7, right).

By analyzing native and non-native contacts with the cpptraj module of the AMBER program, we observed a generally consistent number of total contacts between the receptor and the SHH-N-cholesterol protein lacking 22 amino acid residues at the N-terminus, during the entire MD simulations of the PR-SHH-N-cholesterol and AR-SHH-N-cholesterol complexes, as well as during the last 0.6 μ s of the MD simulation of the ER α -SHH-N-cholesterol complex (Figure S14b). The number of these contacts is similar for all three complexes. In addition, analyses have indicated that the total number of contacts between the receptors and SHH-N protein increases as the simulation progresses, which can be explained by the progressively more stable binding of the N-terminus of SHH-N-cholesterol to the body of the SHR protein. The largest number of contacts observed during the last 600 ns of MD simulations in the ER α -SHH-N-cholesterol (Figure S14a) aligns with the highest binding affinity determined for the complex during this period. (Table 1). At the same time, large fluctuations in the total number of contacts observed for the AR-SHH-N-cholesterol complex agree with the highest flexibility of the SHH-N N-terminus noted for this complex throughout MD simulations (Figure S7, right). Figure 6 illustrates all contacts, encompassing both native and non-native interactions, on the structures of the PP complexes for each amino acid, as calculated during the final 200 ns of the simulations. Notably, it becomes evident that the N- and C-terminal amino acid residues of SHH-N-cholesterol, along with the cholesterol moiety itself, exert the most pronounced impact on PP complex stabilization in all complexes with SHH-N-cholesterol.

According to MM/PBSA binding enthalpies (Table 1), the binding of cholesterol attached to the C-terminus of SHH-N to ER α is more exothermic than the binding of estradiol (-12.87 kcal/mol) or cholesterol alone (-17.50 kcal/mol), which have almost similar binding energies. Apparently, numerous favorable interactions between SHH-N and ER α proteins contribute to more favorable binding of SHH-N-cholesterol to ER α , than estradiol. Interestingly, calculated MM/PBSA binding energies predict similar enthalpies for progesterone (-19.02 kcal/mol), free cholesterol and cholesterol attached to SHH-N C-terminus to PR. Apparently, MM/PBSA analysis predict no significant difference in cholesterol binding to PR when free or attached to SHH-N C-terminus, suggesting a negligible energy contribution of the SHH-N protein body to the formation of the PP complex.

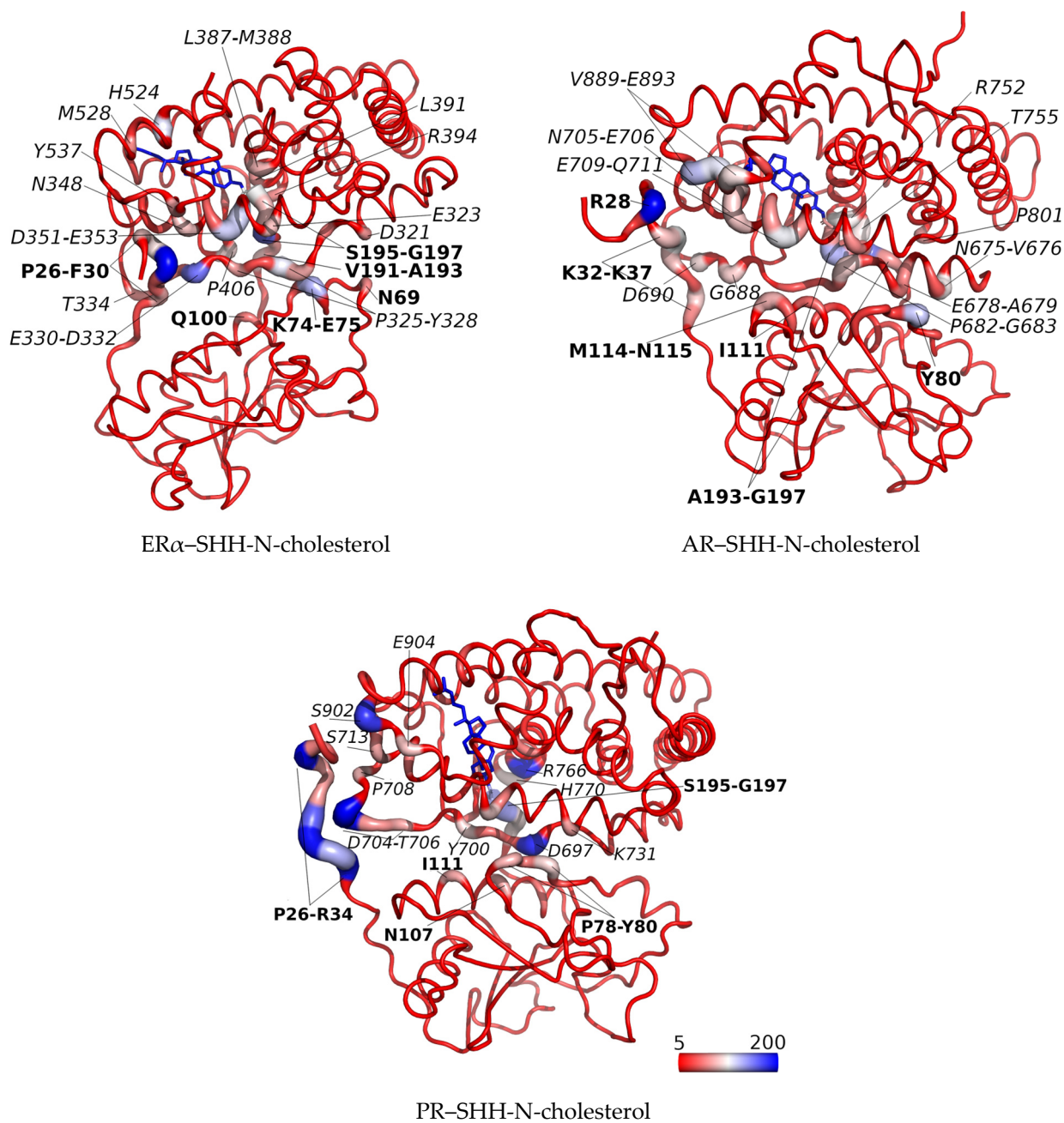


Figure 6. Relative contact strengths for all native and non-native contacts calculated on the last 200 ns of MD simulations (1.8–2.0 μ s in case of ER α -SHH-N-cholesterol, 0.8–1.0 μ s in case of PR-SHH-N-cholesterol complex simulation with lower binding energy determine, and 0.3–0.5 μ s in case of AR-SHH-N-cholesterol) and shown using B-factor putty representation (for protein residues) and/or color coding (protein and cholesterol moiety). Relative contact strengths calculated per atom are summed for each residue and summed values are shown. A red to white to blue colors (with minimum and maximum values set at 5 and 200, respectively) and a narrower to wider tube indicate regions with lower to higher summed relative contact strength. The complex is oriented so that the SHR is at the top and SHH-N is at the bottom of the figure. Amino acids from SHR and SHH-N-cholesterol are indicated in italic and bold, respectively. Cholesterol moiety is shown as sticks. The figures were prepared using the software pymol (The PyMOL Molecular Graphics System, Version 2.3.0 Schrödinger, LLC, New York, NY, USA).

4. Discussion

SHH is a main ligand involved in the canonical activation of the HH-GLI signaling pathway. Mature SHH has cholesterol PTM, which is indispensable for its secretion, spread, and reception [48]. Those processes are accomplished by physical interaction between its cholesterol moiety and two proteins, the membrane-protein-dispatched homolog 1 (DISP1) and a member of the Scube family of secreted-proteins-signal peptide, CUB and EGF-like domain-containing protein 2 (SCUBE2) [49]. Our previous research has provided experimental evidence of a complex formation between the C-terminally cholesteroylated N-terminal domain of SHH and ER α and AR proteins [18,20]. In this study, our main focus was to investigate the potential binding of SHH-N-cholesterol to PR, the only member of the nuclear SHR subfamily not previously associated with SHH-N. Computational methods were utilized to predict the protein-protein binding poses and to assess the stability of the resulting complexes. Docking calculations, followed by robust MD simulations and free energy calculations, predict a stable binding of SHH-N-cholesterol protein with all three SHRs. The values of the PP binding energies suggest that C-terminally cholesteroylated N-terminal domain of SHH binds most strongly with ER α (-51.51 ± 7.30 kcal/mol) protein, and equally strongly with AR (-33.03 ± 10.27 kcal/mol) and PR (-23.25 ± 7.66 or -27.95 ± 7.80 kcal/mol) proteins. These results suggest that a non-canonical interaction between PR and the C-terminally cholesteroylated N-terminal domain of SHH could exist, and consequently, that it could have some biological consequences.

During microseconds-long MD simulations, cholesterol, free or attached to the SHH-N C-terminus, stays tightly bound in the SHRs' binding site. In the complex with ER α or PR it occupies the same position as determined for its natural agonist, estradiol and progesterone, respectively. Interestingly, MM/PBSA calculations (Table 1) predict no significant difference in the binding affinity of PR towards progesterone (-19.02 ± 2.97 kcal/mol), compared to its affinity for SHH-N-cholesterol. On the contrary, in the case of binding with ER α , SHH-N-cholesterol showed a more favorable enthalpy of binding (-51.51 ± 7.30 kcal/mol) with the receptor, compared to estradiol (-12.87 ± 2.68 kcal/mol). Considering the nearly identical binding affinities of ER α towards estradiol and free cholesterol (-17.50 ± 3.42 kcal/mol), it can be inferred that the additional stabilization observed in the ER α -SHH-N-cholesterol complex stems from favorable PP interactions formed between SHH-N and the ER α protein. The per-residue MM/GBSA analysis identified numerous favorable interactions between the unstructured C- and N-termini of SHH-N, along with the more structured central part of the SHH-N protein, and ER α , PR, and AR proteins. The analysis of both native and non-native contacts, along with the examination of hydrogen bonds, highlights a notably greater contribution from the N- and C-terminal residues of SHH-N to the stabilization of the complex with ER α , in contrast to the complexes with PR and especially AR, throughout the course of MD simulations.

The MM/GBSA and hydrogen bond analyses reveal the crucial role of hydrogen bonds and non-polar interactions in stabilizing natural agonists and cholesterol moiety in the binding site of the SHRs. Notably, the contribution of hydrogen bonding is more pronounced in complexes with estradiol and progesterone. These interactions persist even during significant structural rearrangements of protein subunits observed in the MD simulation of the ER α -SHH-N-cholesterol complex.

To summarize, our calculations suggest that the formation of PR-SHH-N-cholesterol complex is theoretically plausible, though experimental verification is still pending and it is something that we are currently working on. Since 30–50% of patients treated with endocrine therapies develop resistance [50], targeting the interaction between SHH-N and SHRs might be a valuable strategy for the treatment of endocrine therapy-resistant tumors.

Supplementary Materials: The following supporting information can be downloaded at: <https://www.mdpi.com/article/10.3390/app14020562/s1>, Figure S1: The SHH structure deposit under PDB code 6RVD; Figure S2: The protein-protein complex structures predicted by Hdock server; Figure S3: Profiles of RMSD, Rg and RMSF for simulated complexes; Figure S4: Binding of the estra-

diol, progesterone or cholesterol (moiety) with SHR during MD simulations; Figure S5: Distances between the oxygen atoms of cholesterol, estradiol, and progesterone, and selected amino acids of SHRs during MD simulations; Figure S6: Distances and hydrogen bonds between selected SHRs' residues located at the entrance to the ligand-binding site; Figure S7: Mutual adjustment of the SHH-N-cholesterol and ER α , PR or AR proteins during MD simulations; Figure S8: Mutual orientation of the protein subunits in the initial structures used for molecular modeling study and the optimized protein-protein complex structures obtained by MD simulations; Figure S9: Superposition of the final AR-SHH-N-cholesterol complexes obtained in our previous publication and in this study; Figure S10: The MM/GBSA per-residue energy decomposition performed for AR and SHH-N-cholesterol in the complex on the 0.5 μ s-long MD trajectory; Figure S11: Binding of cholesterol and cholesterol moiety covalently bounded at C-terminus of SHH-N with SHRs in the optimized structures obtained at the end of MD simulations; Figure S12: Number of hydrogen bonds that selected amino acids of SHH-N and SHR form with the protein binding partner calculated during entire MD simulations; Figure S13: The optimized structures of AR-SHH-N-cholesterol and ER α -SHH-N-cholesterol complexes obtained at the end of MD simulations, with indicated amino acids that participate in protein-protein interaction; Figure S14: Number of native and non-native contact calculated during MD simulations of the complexes.

Author Contributions: Conceptualization, A.T. and P.O.; methodology, A.T.; software, A.T.; validation, A.T., J.Č. and P.O.; formal analysis, A.T.; investigation, A.T., J.Č. and P.O.; resources, A.T.; data curation, A.T.; writing—original draft preparation, A.T., J.Č. and P.O.; writing—review and editing, A.T. and P.O.; visualization, A.T.; supervision, A.T.; project administration, A.T. and P.O. All authors have read and agreed to the published version of the manuscript.

Funding: This research was funded by the Croatian Science Foundation: IP-2018-01-2936. The work of doctoral student J.Č. was supported by the “Young Researchers’ Career Development Project-Training of Doctoral Students”, which was provided by the Croatian Science Foundation (DOK-2021-02-5821).

Institutional Review Board Statement: Not applicable.

Informed Consent Statement: Not applicable.

Data Availability Statement: Data available in a publicly accessible repository. The data presented in this study are openly available in Mendeley Data at doi: 10.17632/jmnp4s5ccx.1 (<https://data.mendeley.com/datasets/jmnp4s5ccx/1>).

Acknowledgments: The authors acknowledge the University Computing Center, University of Zagreb (<https://www.srce.unizg.hr/en/advanced-computing>, accessed 1 May 2023), specifically the Isabella cluster, for the provided computer time.

Conflicts of Interest: The authors declare no conflicts of interest.

References

1. Sigafos, A.N.; Paradise, B.D.; Fernandez-Zapico, M.E. Hedgehog/GLI Signaling Pathway: Transduction, Regulation, and Implications for Disease. *Cancers* **2021**, *13*, 3410. [[CrossRef](#)] [[PubMed](#)]
2. Varjosalo, M.; Li, S.-P.; Taipale, J. Divergence of Hedgehog Signal Transduction Mechanism between Drosophila and Mammals. *Dev. Cell* **2006**, *10*, 177–186. [[CrossRef](#)] [[PubMed](#)]
3. Kurtović, M.; Piteša, N.; Bartoniček, N.; Ozretić, P.; Musani, V.; Čonkaš, J.; Petrić, T.; King, C.; Sabol, M. RNA-Seq and ChIP-Seq Identification of Unique and Overlapping Targets of GLI Transcription Factors in Melanoma Cell Lines. *Cancers* **2022**, *14*, 4540. [[CrossRef](#)] [[PubMed](#)]
4. Dawber, R.J.; Hebbes, S.; Herpers, B.; Docquier, F.; van den Heuvel, M. Differential Range and Activity of Various Forms of the Hedgehog Protein. *BMC Dev. Biol.* **2005**, *5*, 21. [[CrossRef](#)] [[PubMed](#)]
5. Varjosalo, M.; Taipale, J. Hedgehog: Functions and Mechanisms. *Genes Dev.* **2008**, *22*, 2454–2472. [[CrossRef](#)] [[PubMed](#)]
6. Ciepla, P.; Magee, A.I.; Tate, E.W. Cholesterylation: A Tail of Hedgehog. *Biochem. Soc. Trans.* **2015**, *43*, 262–267. [[CrossRef](#)] [[PubMed](#)]
7. Resh, M.D. Palmitoylation of Hedgehog Proteins by Hedgehog Acyltransferase: Roles in Signalling and Disease. *Open Biol.* **2021**, *11*, 200414. [[CrossRef](#)]
8. Musani, V.; Ozretić, P.; Trnski, D.; Sabol, M.; Poduje, S.; Tošić, M.; Šitum, M.; Levanat, S. Potential Hot Spot for de Novo Mutations in PTCH1 Gene in Gorlin Syndrome Patients: A Case Report of Twins from Croatia. *Croat. Med. J.* **2018**, *59*, 20–24. [[CrossRef](#)]
9. Car, D.; Sabol, M.; Musani, V.; Ozretić, P.; Levanat, S. Epigenetic Regulation of the Hedgehog-Gli Signaling Pathway in Cancer. *Period. Biol.* **2010**, *112*, 419–423.

10. Budimir, I.; Tomasović-Lončarić, Č.; Kralik, K.; Čonkaš, J.; Eljuga, D.; Žic, R.; Gorjanc, B.; Tucaković, H.; Caktaš, D.; Jaman, J.; et al. Higher Expressions of SHH and AR Are Associated with a Positive Receptor Status and Have Impact on Survival in a Cohort of Croatian Breast Cancer Patients. *Life* **2022**, *12*, 1559. [[CrossRef](#)]
11. Levanat, S.; Sabol, M.; Musani, V.; Ozretić, P.; Trnski, D. Hedgehog Signaling Pathway as Genetic and Epigenetic Target in Ovarian Tumors. *Curr. Pharm. Des.* **2016**, *22*, 73–94. [[CrossRef](#)]
12. Liao, X.; Siu, M.K.; Au, C.W.; Chan, Q.K.; Chan, H.Y.; Wong, E.S.; Ip, P.P.; Ngan, H.Y.; Cheung, A.N. Aberrant Activation of Hedgehog Signaling Pathway Contributes to Endometrial Carcinogenesis through β -Catenin. *Mod. Pathol.* **2009**, *22*, 839–847. [[CrossRef](#)] [[PubMed](#)]
13. Bushman, W. Hedgehog Signaling in Prostate Development, Regeneration and Cancer. *J. Dev. Biol.* **2016**, *4*, 30. [[CrossRef](#)] [[PubMed](#)]
14. Henderson, B.E.; Feigelson, H.S. Hormonal Carcinogenesis. *Carcinogenesis* **2000**, *21*, 427–433. [[CrossRef](#)] [[PubMed](#)]
15. Rochefort, H.; Chabos, D. The Role of Sex Steroid Receptors on Lipogenesis in Breast and Prostate Carcinogenesis: A Viewpoint. *Horm. Cancer* **2010**, *1*, 63–70. [[CrossRef](#)] [[PubMed](#)]
16. Olefsky, J.M. Nuclear Receptor Minireview Series. *J. Biol. Chem.* **2001**, *276*, 36863–36864. [[CrossRef](#)] [[PubMed](#)]
17. Sever, R.; Glass, C.K. Signaling by Nuclear Receptors. *Cold Spring Harb. Perspect. Biol.* **2013**, *5*, a016709. [[CrossRef](#)] [[PubMed](#)]
18. Sabol, M.; Trnski, D.; Uzarevic, Z.; Ozretic, P.; Musani, V.; Rafaj, M.; Cindric, M.; Levanat, S. Combination of Cyclopamine and Tamoxifen Promotes Survival and Migration of MCF-7 Breast Cancer Cells—Interaction of Hedgehog-Gli and Estrogen Receptor Signaling Pathways. *PLoS ONE* **2014**, *9*, e114510. [[CrossRef](#)] [[PubMed](#)]
19. Miller, W.L.; Auchus, R.J. The Molecular Biology, Biochemistry, and Physiology of Human Steroidogenesis and Its Disorders. *Endocr. Rev.* **2011**, *32*, 81–151. [[CrossRef](#)]
20. Trnski, D.; Sabol, M.; Tomić, S.; Štefanac, I.; Mrčela, M.; Musani, V.; Rinčić, N.; Kurtović, M.; Petrić, T.; Levanat, S.; et al. SHH-N Non-Canonically Sustains Androgen Receptor Activity in Androgen-Independent Prostate Cancer Cells. *Sci. Rep.* **2021**, *11*, 14880. [[CrossRef](#)]
21. Sartorius, C.A.; Melville, M.Y.; Hovland, A.R.; Tung, L.; Takimoto, G.S.; Horwitz, K.B. A Third Transactivation Function (AF3) of Human Progesterone Receptors Located in the Unique N-Terminal Segment of the B-Isoform. *Mol. Endocrinol.* **1994**, *8*, 1347–1360. [[CrossRef](#)] [[PubMed](#)]
22. Hopp, T.A.; Weiss, H.L.; Hilsenbeck, S.G.; Cui, Y.; Allred, D.C.; Horwitz, K.B.; Fuqua, S.A.W. Breast Cancer Patients with Progesterone Receptor PR-A-Rich Tumors Have Poorer Disease-Free Survival Rates. *Clin. Cancer Res.* **2004**, *10*, 2751–2760. [[CrossRef](#)] [[PubMed](#)]
23. Jaffrain-Rea, M.L.; Petrangeli, E.; Ortolani, F.; Fraioli, B.; Lise, A.; Esposito, V.; Spagnoli, L.G.; Tamburrano, G.; Frati, L.; Gulino, A. Cellular Receptors for Sex Steroids in Human Pituitary Adenomas. *J. Endocrinol.* **1996**, *151*, 175–184. [[CrossRef](#)] [[PubMed](#)]
24. Liu, D. Gene Signatures of Estrogen and Progesterone Receptor Pathways Predict the Prognosis of Colorectal Cancer. *FEBS J.* **2016**, *283*, 3115–3133. [[CrossRef](#)] [[PubMed](#)]
25. Vannucchi, G.; De Leo, S.; Perrino, M.; Rossi, S.; Tosi, D.; Cirello, V.; Colombo, C.; Bulfamante, G.; Vicentini, L.; Fugazzola, L. Impact of Estrogen and Progesterone Receptor Expression on the Clinical and Molecular Features of Papillary Thyroid Cancer. *Eur. J. Endocrinol.* **2015**, *173*, 29–36. [[CrossRef](#)] [[PubMed](#)]
26. Elmaogod, E.A.; Khairy, D.; Mahmoud, A. Clinicopathological Role of Progesterone Hormone in IDH-Mutant Astrocytoma. *J. Microsc. Ultrastruct.* **2023**. [[CrossRef](#)]
27. Deli, T.; Orosz, M.; Jakab, A. Hormone Replacement Therapy in Cancer Survivors—Review of the Literature. *Pathol. Oncol. Res.* **2020**, *26*, 63–78. [[CrossRef](#)] [[PubMed](#)]
28. Lin, H.; Lan, K.-C.; Ou, Y.-C.; Wu, C.-H.; Kang, H.-Y.; Chuang, I.-C.; Fu, H.-C. Highly Expressed Progesterone Receptor B Isoform Increases Platinum Sensitivity and Survival of Ovarian High-Grade Serous Carcinoma. *Cancers* **2021**, *13*, 5578. [[CrossRef](#)]
29. Yang, S.; Thiel, K.W.; Leslie, K.K. Progesterone: The Ultimate Endometrial Tumor Suppressor. *Trends Endocrinol. Metab.* **2011**, *22*, 145–152. [[CrossRef](#)]
30. Mukhopadhyay, M.; Das, C.; Kumari, M.; Sen, A.; Mukhopadhyay, B.; Mukhopadhyay, B. Spectrum of Meningioma with Special Reference to Prognostic Utility of ER, PR and Ki67 Expression. *J. Lab. Physicians* **2017**, *9*, 308–313. [[CrossRef](#)]
31. Brzozowski, A.M.; Pike, A.C.W.; Dauter, Z.; Hubbard, R.E.; Bonn, T.; Engström, O.; Öhman, L.; Greene, G.L.; Gustafsson, J.-Å.; Carlquist, M. Molecular Basis of Agonism and Antagonism in the Oestrogen Receptor. *Nature* **1997**, *389*, 753–758. [[CrossRef](#)] [[PubMed](#)]
32. Waterhouse, A.; Bertoni, M.; Bienert, S.; Studer, G.; Tauriello, G.; Gumienny, R.; Heer, F.T.; de Beer, T.A.P.; Rempfer, C.; Bordoli, L.; et al. SWISS-MODEL: Homology Modelling of Protein Structures and Complexes. *Nucleic Acids Res.* **2018**, *46*, W296–W303. [[CrossRef](#)] [[PubMed](#)]
33. Williams, S.P.; Sigler, P.B. Atomic Structure of Progesterone Complexed with Its Receptor. *Nature* **1998**, *393*, 392–396. [[CrossRef](#)] [[PubMed](#)]
34. Rudolf, A.F.; Kinnebrew, M.; Kowatsch, C.; Ansell, T.B.; El Omari, K.; Bishop, B.; Pardon, E.; Schwab, R.A.; Malinauskas, T.; Qian, M.; et al. The Morphogen Sonic Hedgehog Inhibits Its Receptor Patched by a Pincer Grasp Mechanism. *Nat. Chem. Biol.* **2019**, *15*, 975–982. [[CrossRef](#)] [[PubMed](#)]

35. Pereira de Jésus-Tran, K.; Côté, P.; Cantin, L.; Blanchet, J.; Labrie, F.; Breton, R. Comparison of Crystal Structures of Human Androgen Receptor Ligand-binding Domain Complexed with Various Agonists Reveals Molecular Determinants Responsible for Binding Affinity. *Protein Sci.* **2006**, *15*, 987–999. [[CrossRef](#)] [[PubMed](#)]
36. Yan, Y.; Tao, H.; He, J.; Huang, S.-Y. The HDOCK Server for Integrated Protein–Protein Docking. *Nat. Protoc.* **2020**, *15*, 1829–1852. [[CrossRef](#)] [[PubMed](#)]
37. Izadi, S.; Anandakrishnan, R.; Onufriev, A.V. Building Water Models: A Different Approach. *J. Phys. Chem. Lett.* **2014**, *5*, 3863–3871. [[CrossRef](#)]
38. Tian, C.; Kasavajhala, K.; Belfon, K.A.A.; Raguette, L.; Huang, H.; Miguez, A.N.; Bickel, J.; Wang, Y.; Pincay, J.; Wu, Q.; et al. Ff19SB: Amino-Acid-Specific Protein Backbone Parameters Trained against Quantum Mechanics Energy Surfaces in Solution. *J. Chem. Theory Comput.* **2020**, *16*, 528–552. [[CrossRef](#)]
39. Wang, J.; Wolf, R.M.; Caldwell, J.W.; Kollman, P.A.; Case, D.A. Development and Testing of a General Amber Force Field. *J. Comput. Chem.* **2004**, *25*, 1157–1174. [[CrossRef](#)]
40. Tomić, A.; Abramić, M.; Spoljarić, J.; Agić, D.; Smith, D.M.; Tomić, S. Human Dipeptidyl Peptidase III: Insights into Ligand Binding from a Combined Experimental and Computational Approach. *J. Mol. Recognit.* **2011**, *24*, 804–814. [[CrossRef](#)]
41. Loncharich, R.J.; Brooks, B.R.; Pastor, R.W. Langevin Dynamics of Peptides: The Frictional Dependence of Isomerization Rates Of N-Acetylalanyl-N'-Methylamide. *Biopolymers* **1992**, *32*, 523–535. [[CrossRef](#)]
42. Berendsen, H.J.C.; Postma, J.P.M.; van Gunsteren, W.F.; DiNola, A.; Haak, J.R. Molecular Dynamics with Coupling to an External Bath. *J. Chem. Phys.* **1984**, *81*, 3684–3690. [[CrossRef](#)]
43. Salomon-Ferrer, R.; Götz, A.W.; Poole, D.; Le Grand, S.; Walker, R.C. Routine Microsecond Molecular Dynamics Simulations with AMBER on GPUs. 2. Explicit Solvent Particle Mesh Ewald. *J. Chem. Theory Comput.* **2013**, *9*, 3878–3888. [[CrossRef](#)] [[PubMed](#)]
44. Götz, A.W.; Williamson, M.J.; Xu, D.; Poole, D.; Le Grand, S.; Walker, R.C. Routine Microsecond Molecular Dynamics Simulations with AMBER on GPUs. 1. Generalized Born. *J. Chem. Theory Comput.* **2012**, *8*, 1542–1555. [[CrossRef](#)] [[PubMed](#)]
45. Salomon-Ferrer, R.; Case, D.A.; Walker, R.C. An Overview of the Amber Biomolecular Simulation Package. *Wiley Interdiscip. Rev. Comput. Mol. Sci.* **2013**, *3*, 198–210. [[CrossRef](#)]
46. Swanson, J.M.J.; Henchman, R.H.; McCammon, J.A. Revisiting Free Energy Calculations: A Theoretical Connection to MM/PBSA and Direct Calculation of the Association Free Energy. *Biophys. J.* **2004**, *86*, 67–74. [[CrossRef](#)] [[PubMed](#)]
47. Connolly, M.L. Analytical Molecular Surface Calculation. *J. Appl. Crystallogr.* **1983**, *16*, 548–558. [[CrossRef](#)]
48. Siebold, C.; Rohatgi, R. The Inseparable Relationship Between Cholesterol and Hedgehog Signaling. *Annu. Rev. Biochem.* **2023**, *92*, 273–298. [[CrossRef](#)]
49. Tukachinsky, H.; Kuzmickas, R.P.; Jao, C.Y.; Liu, J.; Salic, A. Dispatched and Scube Mediate the Efficient Secretion of the Cholesterol-Modified Hedgehog Ligand. *Cell Rep.* **2012**, *2*, 308–320. [[CrossRef](#)]
50. Rozeboom, B.; Dey, N.; De, P. ER+ Metastatic Breast Cancer: Past, Present, and a Prescription for an Apoptosis-Targeted Future. *Am. J. Cancer Res.* **2019**, *9*, 2821–2831.

Disclaimer/Publisher’s Note: The statements, opinions and data contained in all publications are solely those of the individual author(s) and contributor(s) and not of MDPI and/or the editor(s). MDPI and/or the editor(s) disclaim responsibility for any injury to people or property resulting from any ideas, methods, instructions or products referred to in the content.